Contribution from the Department of Chemistry,
Colorado State University, Fort Collins, Colorado 80523

Electrochemical, Spectral, and Base-Binding Studies of Heterodinuclear Ruthenium–Iron Complexes of *meso*-$\alpha,\alpha,\alpha,\alpha$-Tetrakis(nicotinamidophenyl)porphine

C. Michael Elliott* and J. Kenneth Arnette†

Received January 14, 1986

Electrochemical, spectral, and base-binding studies have been carried out on the heterodinuclear complex $RuCl_2((nic)_4Fe^{III}TPP)Cl$ in DMF solution where $(nic)_4Fe^{III}TPP$ is the ligand (*meso*-tetrakis(*o*-nicotinamidophenyl)porphyrin)iron(III). The $RuCl_2(nic)_4$ moiety has both electronic and steric effects on the iron center. Despite steric restrictions, both the Fe(II) and Fe(III) forms can bind two 1-methylimidazole molecules at the iron center, one occupying the external axial site and one occupying the internal axial site. Additionally, this complex constitutes, to our knowledge, the first solution electrochemical evidence for nitrogen base binding to a Fe(I) porphyrin.

Introduction

Many of the unique properties of metal-containing redox proteins can be directly linked either to steric restriction of the allowable types of coordination at the metal or to interactions of the metal center with other nearby metal sites. In some cases, such as cytochrome oxidase, both factors are important. Herein we report on electrochemical, spectroelectrochemical, and base-binding studies of the complex $RuCl_2((nic)_4Fe^{III}TPP)Cl$ (**3**) where $nic_4Fe^{III}TPP$ is derived from nic_4H_2TPP, the ligand *meso*-tetrakis(*o*-nicotinamidophenyl)porphyrin (**1**).

On the basis of a combination of spectral, electrochemical, and structural information on a large number of analogues (vide infra), the structure of complex **3** can be inferred with a high degree of confidence. The $RuCl_2(nic)_4$ moiety consists of a six-coordinate Ru(II) coordinated to a square-planar arrangement of nicotinamide pyridines and to two Cl^-. The Fe(III) is coordinated in the porphyrin site. The single Cl^- coordinated to Fe(III) is, for steric reasons, most probably coordinated at the external axial site of the iron. Both metals are redox active and the $RuCl_2(nic)_4$ moiety serves as a "cap" to one face of the porphyrin. Consequently, complex **3** has both steric restriction and multiple redox site properties. As a result of these features, **3** and its several oxidation-state variations have properties that are significantly different from those of simple iron porphyrins.

Experimental Methods

Synthesis. The structure of the ligand nic_4H_2TPP (**1**) is given in Figure 1. The syntheses of **1** and $RuCl_2((nic)_4H_2TPP)$, where the Ru is coordinated by the nicotinamide pickets, have been described previously.[1]

$RuCl_2((nic)_4Fe^{II}TPP)$ (2). In an inert-atmosphere box, $RuCl_2((nic)_4H_2TPP)$ (0.100 g), $FeCl_2$ (anhydrous, 1.0 g), and 2,6-lutidine (0.6 mL) were dissolved in 25 mL of *N*,*N*-dimethylformamide (DMF). The solution was gently refluxed for 3 h, and then the solvent was removed under vacuum. The residue was dissolved in 25%/75% nitromethane/tetrahydrofuran (THF), chromatographed on alumina with nitromethane as the eluant, and recrystallized from THF (yield, 15%).

$RuCl_2((nic)_4Fe^{III}TPP)Cl$ (3). $RuCl_2((nic)_4H_2TPP)$ (0.200 g), $FeCl_3$ (anhydrous, 0.50 g) and 2,6-lutidine (1 mL) were dissolved in 40 mL of DMF and refluxed gently under N_2 for 15 h. The solvent was removed by rotary evaporation and the residue dissolved in CH_2Cl_2 with an ultrasonic bath used for stirring. The insoluble $FeCl_3$ was removed by filtration and the solution rotary evaporated to dryness. The porphyrin residue was redissolved in DMF along with LiCl (1.0 g), refluxed for 1 h, and then rotary evaporated to dryness. The residue was dissolved in CH_2Cl_2 and filtered to remove the LiCl. Finally, the product was recrystallized by the addition of methanol to the CH_2Cl_2 solution (yield, 40%). Compound **3** is a single spot on TLC and has a 3:1:1 Cl:Ru:Fe ratio upon X-ray fluorescence analysis.

Spectroscopic and Electrochemical Experiments

Chemicals. Experiments were performed in DMF (Burdick and Jackson, distilled in glass), which was used as obtained. 1-Methylimidazole (1-MeIm, Aldrich) was refluxed over KOH pellets for 3 h and then distilled at reduced pressure. The supporting electrolyte, tetra-*n*-butylammonium hexafluorophosphate ($(TBA)PF_6$), was prepared as described earlier[2] and used at a concentration of 0.1 M.

Equipment. The electrochemical, spectroelectrochemical, and spectrophotometric titration equipment have been described previously.[1,2] All potentials are versus a saturated calomel electrode (SCE).

Electrochemical Titrations. Cyclic voltammetric $E_{1/2}$ potentials were obtained for the Fe(III/II), Fe(II/I), and Ru(II/III) redox couples of **3** as functions of base concentration. The quasi-reversible Fe(II/I) couple data were analyzed according to the method of Kolthoff and Lingane,[3,4] by using the equation

$$(E_{1/2})_c = (E_{1/2})_s - \frac{0.059}{n}\log\left[\frac{\beta^{ox}{}_p}{\beta^{red}{}_q}\right] - \frac{0.059}{n}(p-q)\log[L] \qquad (1)$$

$(E_{1/2})_c$ and $(E_{1/2})_s$ are the half-wave potentials of the complexed and uncomplexed species, respectively. $\beta^{ox}{}_p$ is the overall formation constant for the oxidized complex with p ligands; $\beta^{red}{}_q$ is the overall formation constant for the reduced complex with q ligands. [L] is the concentration of the complexing Lewis base, and n is the number of electrons transferred in the redox reaction.

Spectrophotometric Titrations. Titrations were performed with both **2** (Fe(II)) and **3** (Fe(III)). A 25-mL aliquot of a 0.25 mM solution of **2** in DMF was placed in the titration cell inside the inert-atmosphere box. The cell was then removed briefly to record the initial visible spectrum. Aliquots of pure 1-MeIm or solutions of 1-MeIm in DMF were added to the porphyrin solution inside the inert-atmosphere box via a syringe. After each aliquot, the cell was shaken and allowed to equilibrate before the spectrum was recorded. Following base addition, spectral changes were observed after the initial change (up to 5 min). All absorbances were corrected for dilution.

A similar procedure was followed for the titration of **3**, except that the inert-atmosphere box was unnecessary. A 25-mL aliquot of 0.14 mM solution of **3** in DMF was used in the titration cell. The solution also contained 0.1 M $(TBA)PF_6$ to insure rapid reaction (see below).

The spectral data at low base concentrations were analyzed according to the equation[5]

$$[A - A_0]^{-1} = K_1^{-1}[A_\infty - A_0]^{-1}[L]^{-1} + [A_\infty - A_0]^{-1} \qquad (2)$$

where A is the absorbance at a given wavelength, A_0 is the absorbance of the uncomplexed species, and A_∞ is the absorbance for the fully complexed, monoligated species. K_1 is the formation constant for the mono adduct. Equation 2 applies only to processes in which one ligand is bound or where two ligands are bound but $K_1 \gg K_2$.

By the use of the value of K_1 found from eq 2, the data at all [L] were fit to eq 3 via a general nonlinear least-squares computer program. In

$$A - A_0 = \frac{lT[(\epsilon_1 - \epsilon_0)K_1[L] + (\epsilon_2 - \epsilon_0)\beta_2[L]^2]}{1 + K_1[L] + \beta_2[L]^2} \qquad (3)$$

eq 3, ϵ_0, ϵ_1, and ϵ_2 are the extinction coefficients for the base-free,[6]

† Present address: Shell Development Co., Houston, TX 77001.

(1) Elliott, C. M.; Arnette, J. K.; Krebs, R. R. *J. Am. Chem. Soc.* **1985**, *107*, 4904.
(2) Elliott, C. M.; Hershenhart, E.; Finke, R. G.; Smith, A. L. *J. Am. Chem. Soc.* **1981**, *103*, 5558.
(3) Kolthoff, I. M.; Lingane, J. J. *Polarography*, 2nd ed.; Interscience: New York, 1952; Vol. 1, p 66.
(4) Kadish, K. M.; Bottomley, L. A.; Beroit, B. *Inorg. Chem.* **1978**, *17*, 1124.
(5) Scheidt, W. R.; Lee, Y. J.; Luangdilok, W.; Haller, K. J.; Anzai, K.; Hatano, K. *Inorg. Chem.* **1983**, *22*, 1516.

0020-1669/86/1325-2867$01.50/0

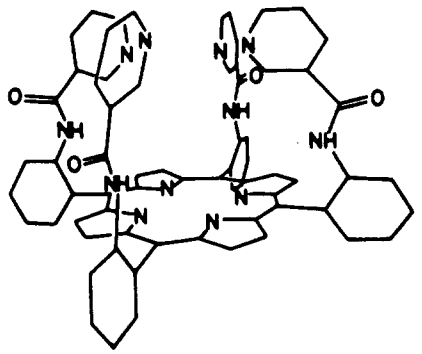

Figure 1. Structure of the ligand $\alpha,\alpha,\alpha,\alpha$-(nic)$_4H_2$TPP (**1**). Double bonds have been removed for clarity.

monoligated, and bisligated species, respectively. The optical cell path length is l, and T is the total porphyrin concentration. Equation 3 was derived from the equation for the total absorbance

$$A = l(\epsilon_0[M] + \epsilon_1[ML] + \epsilon_2[ML_2])$$

(where M is the metalloporphyrin), the equilibrium constant, and the mass balance expressions.

Spectroelectrochemistry. UV–visible spectra were obtained for all accessible oxidation states of **3** in DMF with 0.1 M (TBA)PF$_6$. Small aliquots of neat 1-MeIm were then added to the solution, and the procedure was repeated. In this manner, spectra for each oxidation state as a function of increasing base concentration were obtained.

Results and Discussion

The reactions of RuCl$_2$((nic)$_4$FeTPP)Cl with 1-MeIm display slow kinetics. The speed of reaction appears to depend on the polarity (and/or dielectric constant) of the solvent and the ionic strength of the solution. For example, the reaction of 1-MeIm with **3** in CH_2Cl_2, as followed spectrophotometrically, requires several hours to reach completion; when the same experiment is performed in CH_2Cl_2 with 0.5 M (TBA)PF$_6$, however, the reaction is over in a few minutes. In DMF with 0.1 M (TBA)PF$_6$ the reaction is virtually immediate.

The behavior described above is quite reasonable when one compares **3** with Fe^{III}(TPP)Cl. Sweigart et al.[7] determined that the first molecule of 1-MeIm to bind with Fe^{III}(TPP)Cl attacks the iron center trans to the chloride. Since in **3** the trans position of the iron is hindered, ligand binding must require the predissociation of Cl$^-$. Therefore the ability of the solvent to accommodate, and perhaps even assist, such charge separation will be a major factor in determining the substitution rate.

Due to these kinetic considerations, DMF was chosen as the solvent for the majority of the experiments. Unfortunately, DMF is itself a reasonably good ligand for Fe(II) porphyrins, a fact that complicates the interpretation of measured equilibrium constants. Also, the visible spectra of the DMF and 1-MeIm adducts of **3** are very similar, making the extraction of equilibrium constants from spectral titrations difficult. Despite these problems, it is possible to draw some conclusions about the reactions between **3** and 1-MeIm.

In the following discussion, S refers to a DMF (solvent) molecule and L refers to a 1-MeIm (ligand) molecule. Equilibrium constants are denoted by $K^{a,b}{}_c$/(stepwise) and $\beta^{a,b}{}_c$/(overall), where a is the Ru oxidation state, b is the Fe oxidation state, and c gives the number of ligands L bound to the complex.

Spectrophotometric Titrations. In the analysis of the spectral data, eq 2 was applied to the data at low [L]. The plots of $[A - A_0]^{-1}$ vs. $[L]^{-1}$ were linear for roughly an order of magnitude of [L], after which the experimental points curved away from the calculated lines. The K_1 values were obtained from the low [L] data by dividing the intercept of the $[A - A_0]^{-1}$ vs. $[L]^{-1}$ plot by the slope. These values of K_1 were used as fixed parameters in eq 3, and the remaining coefficients of [L] and $[L]^2$ were allowed to vary by the regression program. The resulting fits were very reasonable at all [L] when compared to the measured $[A - A_0]$ data (vide infra, Figure 3). In principle it is possible to allow all four coefficients in eq 3 to vary during the fitting. However, when this approach was taken several fairly different sets of values were found for the coefficients (local minima), all giving about the same quality of fit. In some cases, physically unreasonable (e.g., negative) values for K_1 or β_2 were obtained. This behavior is probably due to the limited number of experimental points used for the fit. With K_1 fixed, however, the fits were unique, physically meaningful, and consistent with the electrochemical results (see below).

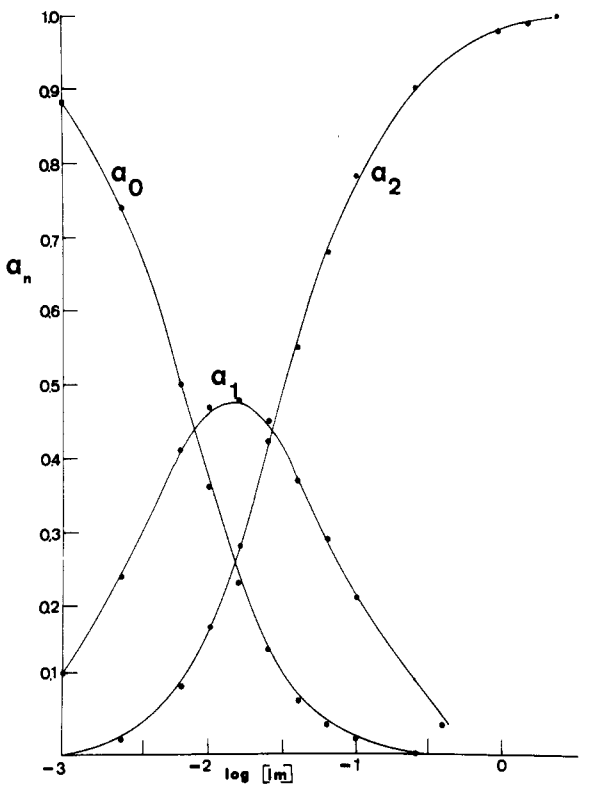

Figure 2. Distributions of Fe(II) (α_0), Fe^{II}L (α_1), and Fe^{II}L$_2$ (α_2) as functions of [1-MeIm].

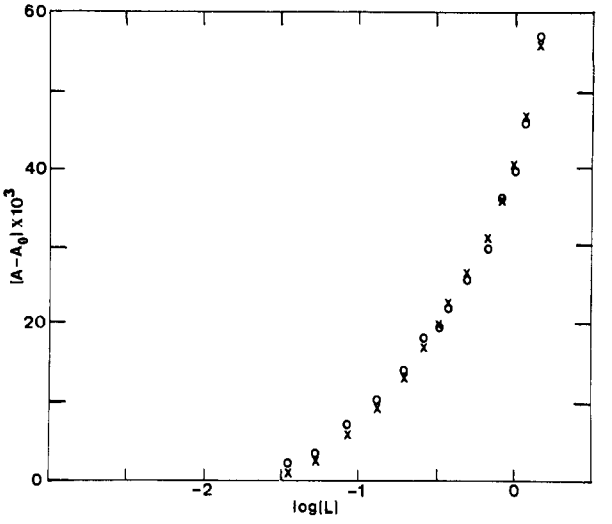

Figure 3. Measured $A - A_0$ (O) and calculated $A - A_0$ (×) values from the fit to eq 3 for the titration of **3**.

Titration of 2 with 1-MeIm. Changes in the visible spectrum of the iron(II) porphyrin with increasing [L] are discussed in the spectroelectrochemistry section below. Isosbestic points and

(6) In this context, base-free means in the absence of 1-MeIm. Both the Fe(II) and Fe(III) species have axial ligands. Fe(II) binds a DMF (solvent) molecule. Comparisons between the CV of **3** in DMF and in CH_2Cl_2 argue strongly that the Cl$^-$ is still coordinated to the iron in DMF. Also the CV behavior of **3** in DMF in the presence of added Cl$^-$ is consistent with the chloride being bound to the iron.

(7) Doeff, M. M.; Sweigart, D. A. *Inorg. Chem.* **1982**, *21*, 3699.

Table I. Isosbestic Points for Titrations of **2** and **3** with 1-MeIm

log [L] range	isosbestic points
$RuCl_2((nic)_4Fe^{II}TPP)$	
−3.00 to −1.26	563
−3.00 to −1.80	515
−2.00 to −0.746	509
$RuCl_2((nic)_4Fe^{III}TPP)Cl$	
−1.74 to −0.732	632, 538, 496, 439
−0.612 to −0.350	622, 543, 490, 437

Table II. Equilibrium Constants of 1-MeIm Binding for Various Oxidation States of **3** and Fe(TPP)Cl

porphyrin complex[a]	log K_1	log K_2	ref
$Ru^{II}Fe^{I}$	1.4		*b*
$Ru^{II}Fe^{II}$	2.10	1.6	*b*
$Ru^{II}Fe^{III}$	0.223	−0.44	*b*
Fe(TPP)Cl	2.10	4.79	9

[a] All measurements were made in DMF solvent. [b] This work.

concentration ranges over which they are maintained are summarized in Table I. Plotting the absorbances at 615 nm according to eq 2 yields a linear relationship for the range $-3.0 < \log [L] < -1.8$ and gives $K^{2,2}{}_1 = 133$ ($\log K^{2,2}{}_1 = 2.12$) for the reaction

$$(P)Fe^{II} + L \overset{K^{2,2}{}_1}{\rightleftharpoons} (P)Fe^{II}L \qquad (4)$$

where P is the porphyrin ligand. The isosbestic at 515 nm also exists in the above-stated concentration range.

Above log [L] = −1.8, the isosbestic at 515 nm shifts to 509 nm and a new, small band arises at 500 nm; also, the absorbance data no longer obey eq 2. Using $K^{2,2}{}_1$ found above and fitting the entire set of data to eq 3, we obtain $\beta^{2,2}{}_2 = 4800$ ($\log \beta^{2,2}{}_2 = 3.7$) and thereby calculate $K^{2,2}{}_2 = 37$ ($\log K^{2,2}{}_2 = 1.6$) for the reaction

$$(P)Fe^{II}L + L \overset{K^{2,2}{}_2}{\rightleftharpoons} (P)Fe^{II}L_2 \qquad (5)$$

Given the limited number of data points (nine) used to obtain $\beta^{2,2}{}_2$, the calculated value should be viewed as only an estimate. Despite this caveat it should be pointed out that the absorbance data *cannot* be fit reasonably by a mechanism involving the binding of only a single base. This fact is true for both the Fe(II) and Fe(III) oxidation states and is consistent with the electrochemical and spectroelectrochemical results presented subsequently.

The binding of a second 1-MeIm ligand by a capped metalloporphyrin has precedent. In our earlier work with the Ru–Co analogue of **2**,[1] we found that in the Ru(III)–Co(III) oxidation state, the complex will bind two molecules of 1-MeIm at the Co center. Additionally, Basolo et al.[8] have reported $\log K_1 = 3.31$ and $\log \beta_2 = 0.77$ for an Fe(II)-capped porphyrin (in toluene solvent) with a pocket size similar to that of **2**. Finally, on the basis of extensive previous studies with **1** and its Ru–Co complex,[1] binding of nitrogenous bases at the *ruthenium* center does not occur. The most reasonable mode for binding of the second 1-MeIm is at the interior axial position of the Fe. While other possibilities cannot be ruled out (e.g., both imidazoles bound at external axial site), they are, in general, less chemically reasonable.

The calculated distributions of the three proposed iron(II) porphyrin species as a function of log [L] are plotted in Figure 2. The equilibrium constants are summarized in Table II.

Titration of 3 with 1-MeIm. Spectra of the various Fe(III) porphyrin complexes are discussed in detail in the spectroelectrochemistry section below; isosbestics are listed in Table I. Treatment of the absorbances at 575 nm according to eq 2 shows a linear region for $-0.9 < \log [L] < -0.38$ and yields $K^{2,3}{}_1 = 1.67$ ($\log K^{2,3}{}_1 = 0.223$) for the reaction

$$(P)Fe^{III}Cl + L \overset{K^{2,3}{}_1}{\rightleftharpoons} [(P)Fe^{III}L]^+Cl^- \qquad (6)$$

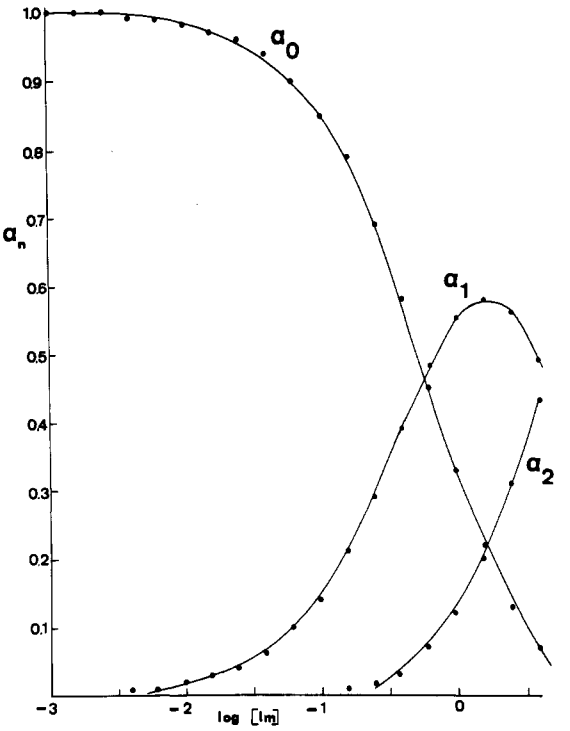

Figure 4. Distributions of Fe(III) (α_0), $Fe^{III}L$ (α_1), and $Fe^{III}L_2$ (α_2) as functions of [1-MeIm].

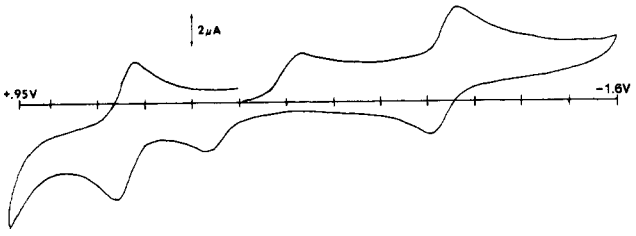

Figure 5. Cyclic voltammogram (vs. SCE) of **3** in DMF solution at a scan rate of 100 mV/s.

As in the titration of Fe(TPP)Cl with 1-MeIm,[9] the presence of the Fe(III) bis adduct is not indicated by the development of a new spectral band but rather by a large shift in the isosbestic points (see Table I). Fitting the absorbance data to eq 3 and using the $K^{2,3}{}_1$ value above yields $\beta^{2,3}{}_2 = 0.61$ ($\log \beta^{2,3}{}_2 = -0.21$). From this result one obtains $K^{2,3}{}_2 = 0.37$ ($\log K^{2,3}{}_2 = -0.44$) for the reaction

$$[(P)Fe^{III}L]^+Cl^- + L \overset{K^{2,3}{}_2}{\rightleftharpoons} [(P)Fe^{III}L_2]^+Cl^- \qquad (7)$$

Again, $\beta^{2,3}{}_2$ (and so $K^{2,3}{}_2$) should be considered an estimate. The values of $(A - A_0)$ calculated from the fit to eq 3 are plotted with the experimental $(A - A_0)$ values in Figure 3. The distribution plots are shown in Figure 4 and the equilibrium constants listed in Table II.

Electrochemistry. Electrochemistry of $RuCl_2((nic)_4FeTPP)Cl$. The cyclic voltammetry wave assignments for **3** (formal oxidation-state assignments) were made by analogy with Fe(TPP)Cl, $Ru(DENA)_4Cl_2$ (DENA = *N*,*N*-diethylnicotinamide[10]), $RuCl_2((nic)_4H_2TPP)$, and $RuCl_2((nic)_4M(TPP))$ ($M = Zn^{+2}$, Cu^{+2}, Ag^{+2}, Ni^{+2}, Mn^{+3}, Co^{+2}). The characteristics of the metal-centered redox couples of **3** in DMF solution are discussed below.

The Ru(II/III) couple is found on the positive scan at $E_{1/2} = 0.487$ V (Figure 5). This is a one-electron, diffusion-controlled, and quasi-reversible process. On the negative scan (Figure 5) the first couple encountered is the Fe(II/III) couple, which is irreversible. The cathodic peak, due to the $(P)Fe^{III}Cl$ reduction, has $E_{p,c} = -0.216$ V while the corresponding anodic peak has $E_{p,a} =$

(8) Ellis, P. E.; Linard, J. E.; Syzmanski, T.; Jones, R. D.; Badge, J. R.; Basolo, F. *J. Am. Chem. Soc.* **1980**, *102*, 1889

(9) Walker, F. A.; Lo, M; Ree, M. T. *J. Am. Chem. Soc.* **1976**, *98*, 5552.

(10) Krebs, R. R. Ph.D. Dissertation, University of Vermont, 1984.

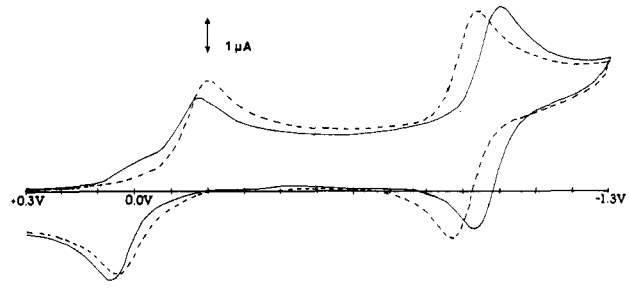

Figure 6. Cyclic voltammograms (vs. SCE) of **3** during titration with 1-MeIm. Dashed line is [L] = 1.1×10^{-2} M; solid line is [L] = 0.13 M.

0.078 V. A small anodic prewave is evident at about −0.13 V and is especially noticeable at slower scan rates. These data suggest that DMF binds to the Fe(II) center much more strongly than to the Fe(III) center, as represented in

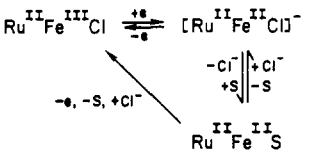

Cyclic voltammetry performed on the system in the presence of added chloride ion verifies that the prewave is due to the oxidation of the $[Ru^{II}Fe^{II}Cl]^-$ species.

The formal Fe(II/I) couple ($E_{1/2}$ = −0.880 V) is a one-electron, diffusion-controlled, and quasi-reversible process. Although this process is probably at least partially ligand-based, it will be referred to here in the formal sense as an Fe(II/I) couple.

Electrochemical Titration of $RuCl_2((nic)_4FeTPP)Cl$ with 1-MeIm. Cyclic voltammograms obtained during the titration were run at a scan rate of 20 mV/s in order to compensate for slow reaction kinetics. By using this slow scan rate and DMF as the solvent, many reaction details are more easily observed than at faster scan rates.

The potential of the Ru(II/III) wave undergoes only small changes during the titration. The $E_{1/2}$ value remains virtually constant at 0.487 V; however, the ΔE_p increases from 88 to 148 mV over the course of the titration.

The Fe(II/I) wave remains chemically reversible throughout the titration (Figure 6), and thus is amenable to analysis by eq 1. The first measurable shift in this wave occurs at log [L] = −3, a 2-fold excess of L. $E_{1/2}$ changes linearly with log [L] in the range −2.0 < log [L] < −1.25 (Figure 7), with a slope of −49.6 mV/log [L]. This slope indicates that, in the given concentration range, the quantity $p - q$ in eq 1 is 1, and thus Fe(II) binds one more molecule of 1-MeIm than does Fe(I). We see from Figure 2 that in the titration of **2**, the predominant solution species for −2 < log [L] < −1.5 is $Fe^{II}L$; we thus conclude that in the electrochemistry for log [L] < −1.25, p = 1 and q = 0 (Fe(I) does not bind). In the neighborhood of log [L] = −1.2, a transition occurs that leads to a second linear region for the range −1.00 < log [L] < 0 (Figure 7). The cyclic voltammograms in the transition region show an isopotential point on the negative side of the Fe(II/I) wave.

The second linear region possesses a slope of −52.6 mV/log [L], which again gives p − q = 1. However, the spectroscopic results (Figure 2) show that above log [L] ≅ −1 the iron(II) porphyrin exists mostly as the bis adduct. It therefore must be concluded that for log[L] > −1.0, p = 2 and q = 1 or that $Fe^{I}L$ exists in solution. The behavior of the Fe(II/I) couple is summarized in the lower right portion of Scheme I.

The intercepts of the two straight lines in Figure 7 are used to calculate equilibrium constants. The intercept, calculated by linear regression, for the low [L] line is −1.004 V. The half-wave potential in the absence of base, $(E_{1/2})_s$, is −0.880 V; from eq 1 we calculate log $K^{2,2}{}_1$ = 2.10 which correlates extremely well with the spectroscopic result of 2.12. The intercept for the high [L] line is −1.015 V, and we find log$[\beta^{2,2}{}_2/K^{2,1}{}_1]$ = 2.29. Using the spectroscopic result for $\beta^{2,2}{}_2$, we calculate log $K^{2,1}{}_1$ = 1.4. This value again is an estimate, since $\beta^{2,2}{}_2$ is not highly accurate (vide supra).

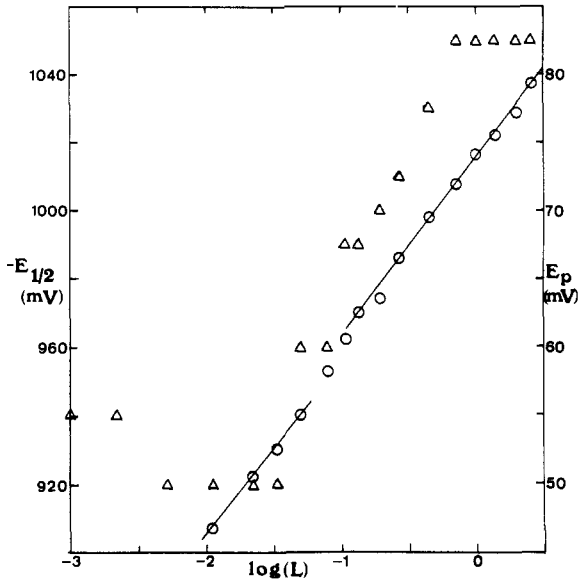

Figure 7. Half-wave potentials ($E_{1/2}$) for the Fe(II/I) couple (O, left axis) and $E_{p,a}$ values for the Fe(II) oxidation wave (Δ, right axis) plotted vs. log [1-MeIm].

Scheme I

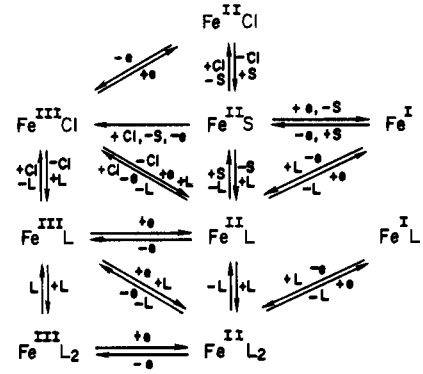

Because the Fe(II/III) couple is irreversible, we cannot rigorously apply eq 1 to the results. We can, however, investigate the behavior of each half of the couple as a function of [L], and in the case of the anodic wave (Fe(II) oxidation) apply eq 1 qualitatively.

The cathodic portion of the Fe(II/III) couple shows a slight positive potential shift at low [L]. At log [L] ≅ −2.3 the wave also begins to shrink. This concentration corresponds to the first significant presence of Fe(III)L in solution as determined spectrophotometrically (Figure 4). As the wave shrinks, it continues to shift in an anodic direction. At higher [L], the wave shrinks more markedly and a new, smaller wave grows in around 0.03 V. The growth of this new wave is shown in Figure 6. Beyond log [L] = 0.16, this new wave ceases to grow and begins to shrink along with the original wave. Figure 4 shows that, at log [L] = 0.16, the Fe(III) bis adduct is beginning to have a significant solution concentration. The cyclic voltammograms as a function of scan rate (Figure 8) show that at high [L] a third broad and ill-defined wave appears around −0.9 V. This wave grows relative to the previous two waves as the scan rate increases. These results are consistent with reactions 6 and 7, rewritten below as

$$(P)Fe^{III}Cl + L \rightleftarrows [(P)Fe^{III}L]^+Cl^- \quad (6a)$$

$$[(P)Fe^{III}L_2]^+Cl^- \rightleftarrows [(P)Fe^{III}L]^+Cl^- + L \quad (7a)$$

At slow scan rates, sufficient time is available for the formation of the mono adduct (reactions 6a and 7a), which is then reduced at a more positive potential. At fast scan rates, the equilibrium distribution among the three porphyrins is "frozen in", and the

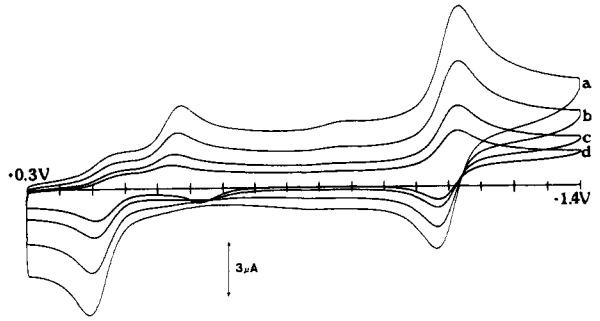

Figure 8. Cyclic voltammograms (vs. SCE) at scan rates of 100 (a), 50 (b), 20 (c), and 10 (d) mV/s for **3** in DMF solution with [1-MeIm] = 1.0 M. The feature at ~−0.23V (reverse scan) is a surface wave, which is present in the background when [1-MeIm] = 1.0 M.

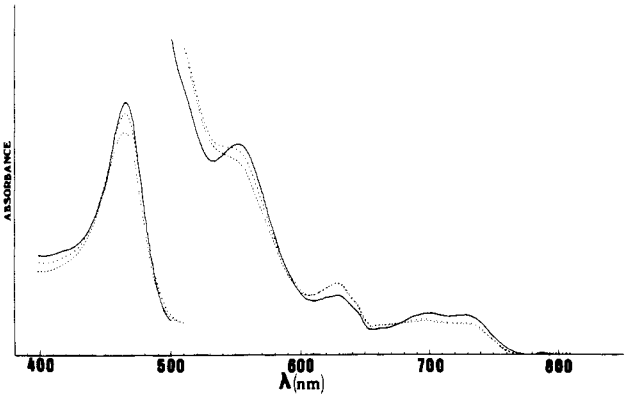

Figure 9. Spectroelectrochemical spectra of Fe(III) (—), $Fe^{III}L$ (···), and $Fe^{III}L_2$ (- - -) in DMF solution with [1-MeIm] = 0.0 M, 6×10^{-3} M, and 1.0 M, respectively.

wave at −0.9 V, corresponding to the reduction of the Fe(III) bis adduct, is observable.

The anodic half of the Fe(II/III) couple shifts negatively in response to increasing [L] until log [L] = −2.3, where $E_{p,a}$ attains a constant value (Figure 7). $E_{p,a}$ is constant until log [L] = −1.5, where it begins to shift back in the positive direction. Thus in the range $-2.3 < \log [L] < -1.5$, $p = q = 1$ for the Fe(II/III) couple. At log [L] = −0.15, $E_{p,a}$ again reaches a constant value, which is maintained for the remainder of the titration. From these results and the spectral titrations, one can conclude that for log [L] > −0.15, $p = q = 2$ for the couple. The interpretation of the behavior of the Fe(II) oxidation wave is consistent with both the spectroscopic and the other electrochemical data. Scheme I depicts the complete reaction scheme for all oxidation states of Fe. Ru(II) has been removed from all species for simplicity, since it appears not to be involved in binding 1-MeIm.

Spectroelectrochemistry. Figures 9–11 show the UV–visible spectra as functions of [L] for the Fe(III), Fe(II), and Fe(I) oxidation states, respectively. Spectra are shown for [L] = 0, 6×10^{-3}, and 1 M, respectively, in each figure. Spectral features are listed in Table III.

The spectra of the Fe(III) state show a Soret band, which decreases in intensity but does not shift as [L] increases. The band at 502 nm flattens for the $Fe^{III}L$ species and finally becomes a shoulder for $Fe^{III}L_2$. These same changes are observed during the spectrophotometric titration.

The Soret band for the Fe(II) species undergoes a red shift and a decrease in intensity with increasing [L]. The Soret for $Fe^{II}L_2$ also has two shoulders on the low wavelength side. In the visible region, the band at 540 nm sharpens and decreases as [L] increases. For $Fe^{II}L_2$, two new bands appear: a very weak band at 495 nm and a small band (previously a shoulder) at 611 nm. The spectral changes agree with those observed during the spectrophotometric titration. It should be pointed out at this time that in none of the oxidation states or ligand-bound forms do the spectra of **3** closely resemble those of other iron porphyrin species. This fact is especially true for the Fe(II) oxidation state. The

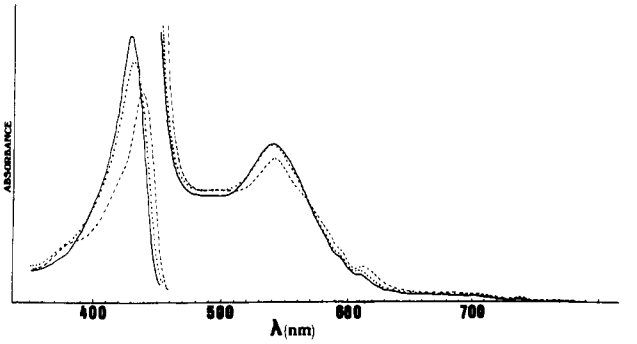

Figure 10. Spectroelectrochemical spectra of Fe(II) (—), $Fe^{II}L$ (···), and $Fe^{III}L_2$ (- - -) in DMF solution with [1-MeIm] = 0.0 M, 6×10^{-3} M, and 1.0 M, respectively.

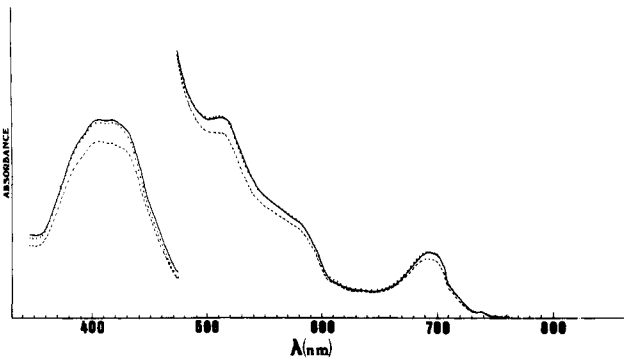

Figure 11. Spectroelectrochemical spectra of Fe(I) in the absence of L (—), Fe(I) at low [L] (···), and Fe(I)L (- - -) in DMF solution. [1-MeIm] = 0.0 M, 6×10^{-3} M, and 1.0 M, respectively.

Table III. Spectral Features of **3** in Its Various Oxidation and Ligand Coordination States

porphyrin complex	λ_{max}, nm
$Ru^{II}Fe^{III}Cl$	415, 465 (sh), 502, 578, 593 (sh), 651, 678
$Ru^{II}Fe^{III}L$	414.5, 500 (sh), 577.5, 592 (sh), 647, 675 (sh)
$Ru^{II}Fe^{III}L_2$	414, 502 (sh), 577.5, 592 (sh), 647, 675 (sh)
$Ru^{II}Fe^{II}S$	430, 540, 555 (sh), 595 (sh), 610 (sh)
$Ru^{II}Fe^{II}L$	432, 540, 594 (sh), 610 (sh)
$Ru^{II}Fe^{II}L_2$	380 (sh), 418 (sh), 437.5, 495, 540, 570 (sh), 594 (sh), 611
$Ru^{II}Fe^{I}$	386 (sh), 405, 417, 430 (sh), 512, 580 (sh), 610 (sh), 691
$Ru^{II}Fe^{I}L$	389 (sh), 405, 418 (sh), 428 (sh), 510 (sh), 580 (sh), 610 (sh), 691
$Ru^{III}Fe^{III}Cl$	417, 507, 578, 594 (sh), 650, 680 (sh)
$Ru^{III}Fe^{III}L$	418, 507, 577, 592 (sh), 650, 680 (sh)

spectral features are distinct. It is thus not possible to use comparison with other known iron porphyrin species to infer the degree of ligand binding and/or oxidation state.

For the formal Fe(I) state, the Soret band is about 2.5 times less intense than that for the Fe(II) state. The spectra for [L] = 0 and [L] = 6×10^{-3} M are effectively identical, showing that there is no binding of 1-MeIm to the formal Fe(I) center for low [L]. The spectrum for [L] = 1.0 M, however, shows subtle changes in the Soret band's shape and a decrease in its intensity, as well as a decrease in the 510-nm shoulder. These changes verify the binding of 1-MeIm at high [L], as indicated by the electrochemical titration.

Conclusion. In view of previous results obtained with $RuCl_2((nic)_4CoTPP)$[1] and with other types of capped porphyrins, the formation of bis(imidazole) adducts with **2** and **3** is not without precedent. In considering the stric restraints imposed in this system it is important to note that $RuCl_2((nic)_4H_2TPP)$ differs from other "capped" systems in several ways. One important feature is that there is very little possibility for lateral motion between the porphyrin plane and the plane formed by the four nicotinamide nitrogens. Examination of molecular models and consideration

of a recently obtained crystal structure of the Ru/Co analogue of **2**[11] indicate that significant variation of the interplanar (and thus the metal-metal) distance can occur upon a screwlike C_4 distortion of the nicotinamide pickets. In the most extended conformation (rigorous C_{4h} symmetry), the metal-metal distance can approach 6 Å. Even in this conformation, normal "end-on" binding of an imidazole within the pocket is not possible due to steric restriction imposed by the chloride bound to the ruthenium at the internal site. Models indicate, however, that with a bent-bonding arrangement an imidazole can be accommodated within the pocket.

Given the steric restraint to one face of the porphyrin imposed by the $RuCl_2(nic)_4$ moiety, the magnitudes of the measured binding constants K_1 and β_2 are plausable for both the II and III oxidation states of iron.

An unusual feature of this complex is that it binds imidazole in the Fe(I) oxidation state. While nitrogenous bases have been demonstrated to bind to Fe(I) porphyrin in frozen solution,[12] we are unaware of any other evidence of nitrogenous base binding to Fe(I) in solution.[13] Because of the almost exact concurrence of the second imidazole binding (ostensibly within the pocket) by Fe(II) with the first binding by Fe(I), it is tempting to speculate that Fe(I) binds its single imidazole within the pocket. The unhindered face of the complex offers an environment that is, to a first approximation, no different from other Fe(I) porphyrins that do not bind nitrogenous bases. The pocket, on the other hand, provides a unique binding site. Irrespective of the exact site of imidazole binding, the behavior of the Fe(I) form of **2** is different from that of other capped and unhindered porphyrins.

Acknowledgment. Support of this work through the U.S. Department of Energy, Division of Chemical Sciences, Special Contract DE-AC02-81ER10968, is gratefully acknowledged.

Registry No. 2, 102648-66-8; **3**, 102648-67-9; $RuCl_2((nic)_4H_2TPP)$, 97232-55-8; $RuCl_2((nic)_4Fe^{I}TPP)$, 102648-68-0; $Ru^{III}Cl_2((nic)_4Fe^{III}TPP)Cl$, 102648-69-1; $Ru^{III}Cl_2((nic)_4Fe^{III}TPP)(1\text{-MeIm})$, 102682-01-9; $RuCl_2((nic)_4Fe^{III}TPP)(1\text{-MeIm})$, 102681-99-2; $RuCl_2((nic)_4Fe^{II}TPP)(1\text{-MeIm})$, 102648-70-4; $RuCl_2((nic)_4Fe^{I}TPP)(1\text{-MeIm})$, 102648-72-6; $RuCl_2((nic)_4Fe^{II}TPP)(1\text{-MeIm})_2$, 102648-71-5; $RuCl_2((nic)_4Fe^{III}TPP)(1\text{-MeIm})_2$, 102682-00-8.

(11) Elliott, C. M.; Redepenning, J. G.; Anderson, O. P.; Schauer, C. K., unpublished results. From this analogous structure we can infer that the arrangements of Cl ions in **3** are as presented, namely a linear arrangement, Cl-Ru-Cl-Fe-Cl.

(12) Srivatsa, G. S.; Sawyer, D. T.; Boldt, N. J.; Bocian, D. F. *Inorg. Chem.* **1985**, *24*, 2125.

(13) Kadish, K. M. In *Iron Porphyrins*; Lever, A. B. P., Gray, H. B., Eds.; Addison-Wesley: Reading, MA, 1983; Vol. 2, p 163 et seq.

Contribution from the Dipartimento di Chimica Inorganica, Metallorganica ed Analitica, University of Padova, and Istituto di Chimica e Tecnologia dei Radioelementi del CNR, Padova, Italy, Laboratoire de Physique Quantique, Université P. Sabatier, Toulouse, France, and Dipartimento di Chimica Inorganica e Struttura Molecolare, University of Messina, Messina, Italy

UV PE Spectra and Pseudopotential ab Initio Calculations on *trans*-$Pt(PEt_3)_2X_2$ Complexes (X = Cl, Br, I)

Giovanni Zangrande,[1a] Gaetano Granozzi,*[1a] Maurizio Casarin,[1b] Jean-Pierre Daudey,[1c] and Domenico Minniti[1d]

Received October 16, 1985

The He I/He II excited photoelectron spectra of *trans*-$Pt(PEt_3)_2X_2$ complexes (X = Cl, Br, I) are fully assigned with the aid of pseudopotential extended basis set ab initio calculations (including relativistic corrections for the Pt atom) on the whole series studied. Electronic reorganization energies upon ionization were estimated by means of a first-order perturbative treatment, which was revealed to be sufficiently accurate to allow a consistent interpretation of the experimental data. Moreover, the ab initio results provided new and interesting results that help to clarify the bonding scheme and its variation along the halide substituent series.

Introduction

Great attention has been focused on Pd(II) and Pt(II) square-planar (d^8) complexes[2] because of their catalytic[3] and anticancer[4] properties. However, despite the large number of investigations, many important features of their chemistry have not yet found an adequate understanding in terms of structure-activity correlations. Actually, definitive evidence concerning their electronic structures, on both experimental and theoretical grounds, is still lacking. Even the energy ordering of occupied molecular orbitals (MOs) and the nature of metal-ligand interactions still present open questions.

Aiming to clarify some of these arguments, we afforded the study of the electronic structures of some tetracoordinated planar complexes of Pd(II) and Pt(II) with simple monodentate ligands.[5] The present paper is devoted to *trans*-$Pt(PEt_3)_2X_2$ derivatives (X = Cl, Br, I), while related alkyl-substituted and hydrido compounds will be discussed in a subsequent paper.

The theoretical study of electronic structures of transition-metal compounds needs a rigorous MO approach, as provided by ab initio calculations, to take into due account bond covalency. This implies going beyond the simple atoms-in-molecule approach typical of early crystal field theory, which is still used to interprete UV-vis spectroscopic data. On the other hand, from the experimental point of view UV-photoelectron (PE) spectroscopy is by far the most direct tool to study the valence monoelectronic levels. However, two major problems must be examined to properly relate experimental PE evidence and theoretical results in a consistent way. First of all one has to override the computational problem arising from the large number of electrons to be included in the SCF procedure. In this regard we have adopted the well-known pseudopotential formalism,[6] so reducing the problem to few valence

(1) (a) University of Padova. (b) CNR. (c) Université P. Sabatier. (d) University of Messina.

(2) (a) Hartley, F. R. *The Chemistry of Platinum and Palladium*; Wiley: New York, 1973. (b) Belluco, U. *Organometallic and Coordination Chemistry of Platinum*; Academic: London, 1974.

(3) Bishop, K. C., III. *Chem. Rev.* **1976**, *76*, 461.

(4) Prestayko, A. W., Crooke, S. T., Carter, S. K., Eds. *Cisplatin: Current Status and Developments*; Academic: New York, 1980.

(5) Granozzi, G.; Zangrande, G.; Bonivento, M.; Michelon, G. *Inorg. Chim. Acta* **1983**, *77*, L229.

0020-1669/86/1325-2872$01.50/0